The persistence of waterfalls in fractured rock

Michael P. Lamb[†] **and William E. Dietrich**
Department of Earth and Planetary Science, University of California, Berkeley, California 94720, USA

ABSTRACT

Although the upstream translation of waterfalls is often thought to occur by undercutting of resistant strata, collapse, and headwall retreat (e.g., Niagara Falls), many propagating waterfalls maintain a vertical face in the absence of undercutting. To explain this observation, we propose that bedrock-fracture geometry exerts a fundamental control on knickpoint morphology and evolution such that vertical waterfalls can persist during retreat due to toppling in bedrock with near horizontal and vertical sets of joints (e.g., columnar basalt). At a waterfall, rock columns are affected by shear and drag from the overflowing water, buoyancy from the plunge pool at the foot of the waterfall, and gravity. We used a torque balance to determine the stability of a rock column and any individual blocks that comprise the column. Results indicate that rotational failure should occur about the base of a headwall (and therefore preserve its form during upstream propagation) where columns are tilted in the downstream direction or slightly tilted in the upstream direction, depending on the plunge-pool depth. Flume experiments were performed to test the model, and the model provides a good prediction of the flow necessary to induce toppling and the morphology of the headwall. Waterfall-induced toppling explains the morphology of canyon headwalls in the volcanic terrain of the northwestern United States, where catastrophic paleofloods (e.g., Bonneville Flood) have carved steep amphitheater-headed canyons in columnar basalt. This model may also explain similar landforms elsewhere on Earth and Mars, and it can be used to predict the minimum flow discharge needed to create these features.

Keywords: knickpoint, amphitheater, plucking, toppling, bedrock erosion, Mars.

[†]Current address: Division of Geological and Planetary Sciences, California Institute of Technology, Pasadena, California 91125, USA
E-mail: mpl@gps.caltech.edu

INTRODUCTION

The upstream propagation of steepened reaches in bedrock rivers (i.e., knickpoints) is one of the fundamental drivers of landscape evolution in hilly and mountainous terrain. Where knickpoints are near vertical, waterfalls form and in some cases can maintain their form while propagating upstream. Why do some waterfalls persist rather than decline in height or rotate as they propagate upstream? To answer this question, some researchers have adapted fluvial-erosion models based on bed stress, stream power, or saltating sediment to explore the development and translation of knickpoints (Howard et al., 1994; Seidl et al., 1994; Whipple and Tucker, 2002; Bishop et al., 2005; Chatanantavet and Parker, 2005; Wobus et al., 2006; Berlin and Anderson, 2007; Crosby et al., 2007; Gasparini et al., 2007). Although these approaches can produce an upstream-propagating wave in the landscape, they do not explicitly model the erosion processes that occur at a waterfall. More process-based models involve undercutting or undermining of the waterfall headwall from either plunge-pool erosion (Stein and Julien, 1993; Bennett, 1999; Alonso et al., 2002; Stein and LaTray, 2002; Flores-Cervantes et al., 2006) or seepage erosion (Howard and McLane, 1988; Dunne, 1990; Lobkovsky et al., 2007; Luo and Howard, 2008). The most well-known example is probably Niagara Falls, where a more resistant limestone cap rock appears to be progressively undercut by plunge-pool erosion, leading to collapse and upstream propagation of the waterfall (Gilbert, 1907).

Although undermining models can explain the persistence of some waterfalls, many waterfalls exist that are not undercut (Von Engeln, 1940; Young, 1985). Many waterfalls also lack the prominent strong-over-weak stratigraphy that allows a vertical headwall to persist in weakly cohesive sediment (Holland and Pickup, 1976; Gardner, 1983). The undermining model has even been questioned for Niagara Falls, where progressive breakdown of the exposed bedrock face might be limiting headwall retreat instead of plunge-pool erosion (Philbrick, 1970, 1974). A rock-breakdown control on the rate of waterfall propagation has also been suggested for retreating waterfalls in Australia (Seidl et al., 1996; Weissel and Seidl, 1997) and Kaua‘i, Hawai‘i (Seidl et al., 1994, 1997). On Kohala, Hawai‘i, others have suggested that headwalls persist and retreat upstream in the absence of undercutting due to continual generation of stepped waterfalls and downward abrasion by gravel transport (Howard et al., 1994; Lamb et al., 2007). Although seepage erosion has been offered as an alternative to plunge-pool erosion (Kochel et al., 1985; Laity and Malin, 1985; Baker, 1990; Pederson, 2001), evidence in support of seepage erosion in bedrock is often ambiguous (Craddock and Howard, 2002; Lamb et al., 2006), and seepage flow is often incompetent to excavate collapsed debris away from the headwall (Lamb et al., 2006, 2007, 2008).

Whereas most landscape-evolution models treat bedrock as homogeneous (e.g., Howard et al., 1994; Whipple and Tucker, 2002; Berlin and Anderson, 2007), the mechanics of waterfall erosion appear to be strongly controlled by bedrock strength, jointing, and stratigraphy (Young, 1985; Miller, 1991; Weissel and Seidl, 1997; Stein and LaTray, 2002; Frankel et al., 2007). Riverbed erosion by abrasion or plucking in general depends on rock strength and joint orientations and spacings (Annandale, 1995; Hancock et al., 1998; Whipple et al., 2000; Coleman et al., 2003; Wohl, 2008). In bedrock with pervasive vertical joints, it has been suggested that waterfalls might retreat due to toppling of rock columns in the absence of undercutting (Young, 1985; Seidl et al., 1996; Weissel and Seidl, 1997). Such waterfalls may be associated with particular geologic settings where bedding or foliation planes have been tilted to near vertical (Weissel and Seidl, 1997; Frankel et al., 2007), or in volcanic terrains where flood basalts develop cooling joints (i.e., columnar basalt) (Young, 1985; O’Connor, 1993; Lamb et al., 2008). For example, Weissel and Seidl (1997) showed clear evidence of toppled columns at the headwall of Apsley River Gorge, Australia, where subvertical joints in metasedimentary rocks promote rotational failure. Near-vertical fracturing also might be expected around bedrock canyons in noncompressive tectonic settings due to

GSA Bulletin; July/August 2009; v. 121; no. 7/8; p. 1123–1134; doi: 10.1130/B26482.1; 9 figures; 1 table.

For permission to copy, contact editing@geosociety.org
© 2009 Geological Society of America

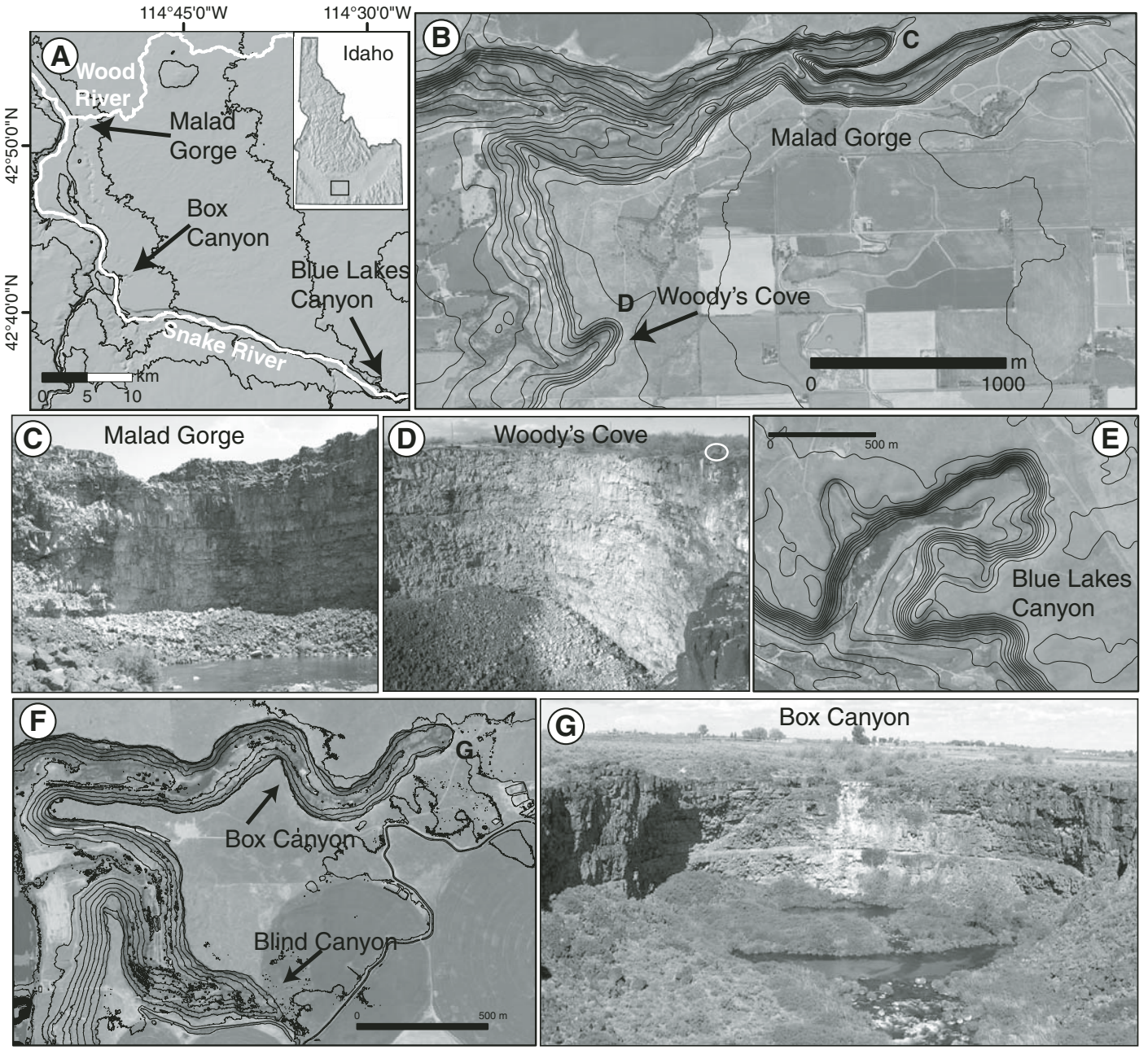

Figure 1. (A) Shaded relief map of the central part of the Snake River Plain, Idaho, showing the locations of three canyons with steep headwalls: Malad Gorge, Box Canyon, and Blue Lakes Canyon. The 30-m-resolution topographic data are from the U.S. Geological Survey. The black lines are 100 m contours. The inset map shows the study location in central Idaho, USA. (B) Shaded relief map of Malad Gorge. C and D labels show the location of the canyon heads in the following photographs. The 10-m-resolution topographic data and 1-m-resolution orthophotograph are from the U.S. Geological Survey. The black lines are 10 m contours. (C) Photograph of one of the heads of Malad Gorge. The headwall relief is ~50 m. (D) Photograph of the head of Woody's Cove. A person for scale is circled in the upper right. (E) Shaded relief map of Blue Lakes Canyon. The 10-m-resolution topographic data and 1-m-resolution orthophotograph are from the U.S. Geological Survey. The black lines are 10 m contours. (F) Shaded relief map of Box and Blind Canyons. G label shows the location of the canyon head in the following photograph. The 1-m-resolution airborne laser-swath mapping data were collected by the National Center for Airborne Laser Mapping, and the 1-m-resolution orthophotograph is from the U.S. Geological Survey. (G) Photograph of the headwall of Box Canyon. The headwall relief is ~35 m. All topographic data are projected onto UTM 11N with NAD83 datum.

topographically induced stresses (Miller and Dunne, 1996). A significant motivation for our study is to better understand how, in volcanic terrains, large paleofloods have rapidly carved canyons with near-vertical, amphitheater-shaped headwalls without significant undercutting (e.g., Lamb et al., 2006, 2008). Two prominent examples are Dry Falls from the Missoula Floods of Washington State, USA (Bretz, 1923; Baker, 1973) and Asbyrgì Canyon, Iceland (Tómasson, 1973). Moreover, large canyons with steep headwalls are abundant on the surface of Mars (e.g., Baker, 1982), and these might also have been cut into columnar basalt by large floods.

In this paper, we explore the hypothesis that waterfalls can persist in the absence of undercutting where river flows generate drag forces sufficient to induce toppling in fractured rock and transport collapsed debris away from the headwall. First, we present a model that balances torques on a rock column. This model reveals that a vertical headwall is likely to be maintained during upstream waterfall propagation where columns are tilted in the downstream direction or slightly tilted in the upstream direction. The model also can be used to estimate the flow discharge needed to cause toppling and headwall retreat. Second, predictions are compared to experiments where stacked bricks failed in a laboratory flume. Finally, we discuss the implications of this work for canyons cut into columnar basalt on Earth and Mars. In particular, we focus on several canyons in the Snake River Plain of Idaho, United States, that have been cut by large paleofloods into columnar basalt (Fig. 1). These include Blue Lakes Canyon, a cataract of the Bonneville Flood (Malde, 1968; O'Connor, 1993), Box Canyon, cut by a paleoflood ca. 45 ka (Lamb et al., 2008), and Malad Gorge, cut by the Wood River (Kauffman et al., 2005) (Fig. 1).

TORQUE-BALANCE MODEL

We develop our model for a bedrock headwall with three perpendicular joint sets, where two are normal to the land surface and the other is parallel to the land surface (Figs. 2 and 3). For convenience, these joint sets will be referred to as vertical and horizontal joints herein. In columnar basalt, for example, these could be contraction cooling joints and bedding planes, respectively (e.g., Aydin and DeGraff, 1988; Budkewitsch and Robin, 1994). For simplicity, we assume that vertical joints extend unimpeded through horizontal joints and vice versa, essentially creating bedrock columns that are composed of individual blocks stacked on top of one another (Fig. 2). We also make the important simplifying assumption that the fracture-bound blocks are free standing and not interlocked with neighboring columns. We discuss the limitations of this approach in the Discussion section. Despite these simplifications, we hypothesize that the geometry used here should be applicable to many landscapes where jointing is pervasive because there should be a high probability that some joints align and are sufficiently wide that they outline free-standing rock columns. This seems to be reasonable based on our field observations of extensive vertical joints with large centimeter-scale joint diameters in flood basalts exposed within the Snake River Plain, Idaho (Fig. 1).

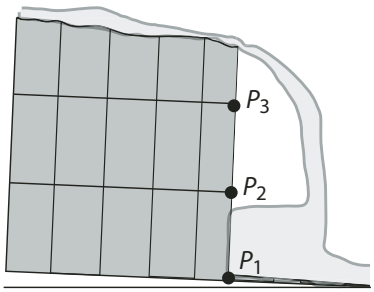

Figure 2. Schematic cartoon showing fractured basalt and three potential points for rotational failure. Two perpendicular joint sets are shown in the schematic, and the third is parallel to the page.

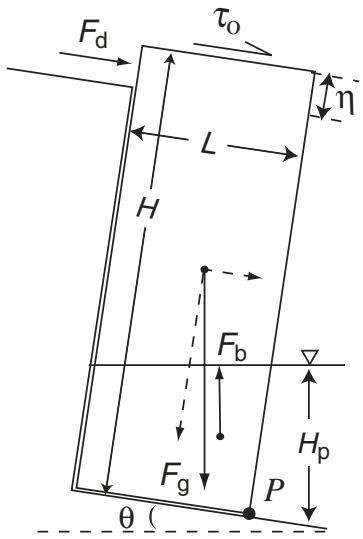

Figure 3. Schematic showing the forces on a rectangular column of rock. See text and notation list for details.

To begin, we first balance the forces and torques caused by flow across a single column of rock at a waterfall lip (Fig. 3). Gravity tends to hold a column in place, whereas it is destabilized by shear and drag from overspilling water and buoyancy produced by the plunge pool at the base of the headwall. Pressure due to heightened pore-fluid levels between rock columns is neglected here, but it is considered in the Discussion section. After balancing torques on a single rock column, we next consider the likely possibility that a column is composed of several blocks stacked vertically on top of one another (Fig. 2). We use the torque-balance model to investigate the conditions where an entire column is more likely to fail than any given block that comprises the column. Where this is the case, a steep headwall is likely to persist during upstream waterfall retreat.

Subject to sufficient force at the top of a rock column, it might fail by either sliding or toppling. Larger aspect ratios of block height (H) to width (L) favor toppling over sliding (Terzaghi, 1962; Goodman and Bray, 1977). For blocks of the same mass and volume, taller blocks have a larger torque arm (Fig. 3), increasing the likelihood of toppling, and a larger normal stress and frictional resistance at their base, decreasing the likelihood of sliding. For example, if roughness within a joint is parameterized using a friction angle of 45°, toppling is favored for $H/L > 0.5$ (Selby, 1993). In this paper, we limit our analysis to blocks or columns that have sufficiently large aspect ratios (or high basal friction) so that failure occurs by toppling, not sliding.

The forces per unit width due to gravity F_g, buoyancy F_b, shear F_s, and drag F_d acting on a column of rock (Fig. 3) can be calculated as

$$F_g = \rho_r g L H, \tag{1A}$$

$$F_b \approx \rho g L H_p, \tag{1B}$$

$$F_s = \tau_o L, \tag{1C}$$

$$F_d = \frac{1}{2}\rho C_d U_\eta^2 \eta, \tag{1D}$$

where ρ_r and ρ are the densities of rock and water, respectively, g is the acceleration due to gravity, τ_o is the boundary shear stress at the top of the column at the overfall lip, C_d is a drag coefficient of order unity (Batchelor, 1967), U_η is the velocity of the flow spatially averaged over the area of the column (per unit width) that protrudes into the flow a distance η, and H_p is the depth of the plunge pool. In formulating the buoyancy force, we have neglected the orientation difference between the submerged portion of the rock column and the free surface of the plunge pool, which tends to be perpendicular to gravity. This was done because it greatly

simplifies the torque balance that follows (e.g., because the center of buoyancy changes as a function of plunge-pool height) and because we found that accounting for this orientation difference had a relatively small effect on the model predictions.

The resulting torques (per unit width) that produce rotation about the pivot point P_1 (Fig. 3) can be calculated from the product of these forces and a representative torque arm:

$$T_g = \frac{1}{2} F_g L \cos\theta \left(1 - \frac{H}{L}\tan\theta\right), \quad (2A)$$

$$T_b \approx \frac{1}{2} F_b L, \quad (2B)$$

$$T_s = F_s H, \quad (2C)$$

$$T_d = F_d H. \quad (2D)$$

To assess stability, we define a factor of safety (FS) as the ratio of resisting to driving torques as

$$FS = \frac{T_g - T_b}{T_s + T_d}. \quad (3)$$

Therefore, where $FS \leq 1$, a column is predicted to fail, and where $FS > 1$, a column is stable. Combining Equations 1, 2, and 3 results in

$$FS = \frac{\frac{\rho_r}{\rho}\cos\theta\left(1 - \frac{H}{L}\tan\theta\right) - \frac{H_p}{H}}{\frac{\tau_o}{\rho g L}\left(2 + \frac{\rho C_d U_\eta^2}{\tau_o}\frac{\eta}{L}\right)}, \quad (4)$$

which can be used to predict the stability of a single column of rock.

In many cases in nature, a column of rock is actually composed of multiple stacked blocks separated by horizontal joints or bedding planes (Fig. 2). In order for a vertical headwall to persist during upstream propagation, the entire column must fail before any given block contained within the column. For example, is toppling failure more likely to occur in Figure 2 about pivot point P_1, P_2, or P_3? If toppling occurs about point P_2 or P_3, then one might expect the headwall to diminish in height over time or evolve into a stair-step pattern. Alternatively, if failure occurs about P_1, then the vertical headwall should persist during upstream propagation. To assess the relative stability of a stack of blocks, we let the height of a block (H_γ) above any arbitrary pivot point be $H_\gamma = \gamma H$, where $0 \leq \gamma \leq 1$. For example, in Figure 2, $\gamma \approx 2/3$ for rotation about P_2 and $\gamma \approx 1/3$ for P_3. The factor of safety for a block of height H_γ (FS_γ) normalized by the factor of safety for the entire column (i.e., Eq. 4) can be written as

$$\frac{FS_\gamma}{FS} = \frac{\frac{\rho_r}{\rho}\cos\theta\left(1 - \frac{\gamma H}{L}\tan\theta\right) - \frac{H(\gamma - 1) + H_p}{\gamma H}}{\frac{\rho_r}{\rho}\cos\theta\left(1 - \frac{H}{L}\tan\theta\right) - \frac{H_p}{H}}, \quad (5)$$

where $H(\gamma - 1) + H_p \geq 0$ accounts for the fact that the elevation of the plunge pool is measured from the base of the column.

Inspection of Equation 5 reveals that the relative stability of any given block in the column is a function of the initial tilt angle of the column ($\tan\theta$) and the plunge-pool height (H_p). For example, if the buoyancy force is negligible (i.e., $H_p = 0$) and a column is perfectly level ($\tan\theta = 0$), then relative stability does not depend on block height, $FS_\gamma/FS = 1$, and failure is predicted to be equally likely at any pivot point. This is because both the torque induced by the overflowing water (which destabilizes the column) and the weight of the column (which adds stability) depend linearly on block height. For conditions where the column is tilted upstream (i.e., $\tan\theta < 0$) and $H_p = 0$, the uppermost block (i.e., small γH) is predicted to be less stable than any taller block, including the entire column (i.e., $FS_\gamma/FS < 1$). During upstream propagation, this should result in breakdown of the vertical headwall. Alternatively, a downstream tilt angle ($\tan\theta > 0$) favors toppling of the entire column over any given block (i.e., $FS_\gamma/FS > 1$), which would allow the vertical headwall to persist during upstream propagation.

The relative stability of the column is also predicted to be a function of the plunge-pool height. Where $0 < H_p < H$, a greater portion of the entire column is submerged than any block higher up, which results in a larger destabilizing buoyancy force acting on the entire column. Where $H_p > H$, the entire column is submerged, and therefore the buoyancy force affects all blocks equally.

Equation 5 implies that vertical headwalls can persist in the absence of undercutting in fractured rock where columns are tilted in the downstream direction, or where slightly tilted upstream if $0 < H_p < H$. This might often be the case for canyons cut into columnar basalt, where canyon-carving floods would follow the same topographic gradient as the lava flows that preceded them, and near-vertical joints (e.g., due to cooling) tend to open perpendicular to the land surface (e.g., Budkewitsch and Robin, 1994). These predictions are explored in more detail next by comparing them to results from flume experiments.

FLUME EXPERIMENTS

Experimental Setup and Methods

Experiments were performed in a 5-m-long, 30-cm-wide flume at the Richmond Field Station of the University of California to test the predictions of the toppling model. The flume could tilt from –2% to 10% slope, and the discharge was adjustable using a variable frequency–controlled pump. A backward-facing, 19.2-cm-high, vertical step was installed ~2 m from the inlet of the flume, creating a waterfall in the flume (Fig. 4). The flume bed and waterfall were made of wood and were relatively smooth. To prevent development of a zone of low air pressure behind the waterfall (e.g., Chanson, 2002), a false wall narrowing the flume width to 27 cm was installed upstream, but not downstream, of the waterfall. Thus, as water poured over the step, it separated not only from the vertical wall below but also from the sidewall, allowing the air pocket beneath the falling water to remain at atmospheric pressure.

Clay bricks of three different thicknesses (L = 3 cm, 6 cm, and 9.7 cm) and a saturated density (ρ_r = 2240 kg/m^3) were used to simulate bedrock columns. These bricks were placed just downstream of the step with their long dimension (19.5 cm) parallel to the width of the flume and their short dimension (i.e., L) parallel to the length of the flume (Fig. 4). The bricks were 9.7 cm in height, and two bricks were stacked on top of one another to create a total column height of H = 19.4 cm. Only one column of bricks (i.e., two bricks in total) was analyzed per experiment. The orientations were intentionally chosen for large H/L to encourage toppling over sliding. Within the flume, the bricks were placed on a piece of sheet metal that could be tilted to change the angle of the brick relative to horizontal (θ) and raised to adjust the distance the bricks protruded above the step (η) (Fig. 3).

For a set flume-bed slope ($S = \tan\beta$, where β is the angle between the floor of the flume and horizontal), brick angle (θ) and protrusion height (η), the discharge of flow was increased stepwise by ~0.7 L/s, pausing for ~90 s between adjustments, until the bricks toppled (Fig. 3B). This time scale was chosen to be significantly longer than the time scale of turbulent eddies (e.g., $\approx h/[\tau_o/\rho]^{1/2}$, where h is the flow depth). The results in Table 1 are classified based on whether the top brick failed or the entire column toppled, as in Figure 4B. The plunge-pool depth (H_p) and flow depth (h) were measured using a ruler.

Each experiment was designed to include a significant component of drag by setting $\eta > 0$ because the shear force alone was not sufficient to induce toppling within the discharge constraints of the flume. For most experiments η/h was small (Table 1), and the protruding column did not affect the overflowing water or the development of the plunge pool (e.g., Fig. 4). This was not true, however, for the experiments with the widest bricks (L = 9.7 cm) where η needed to be

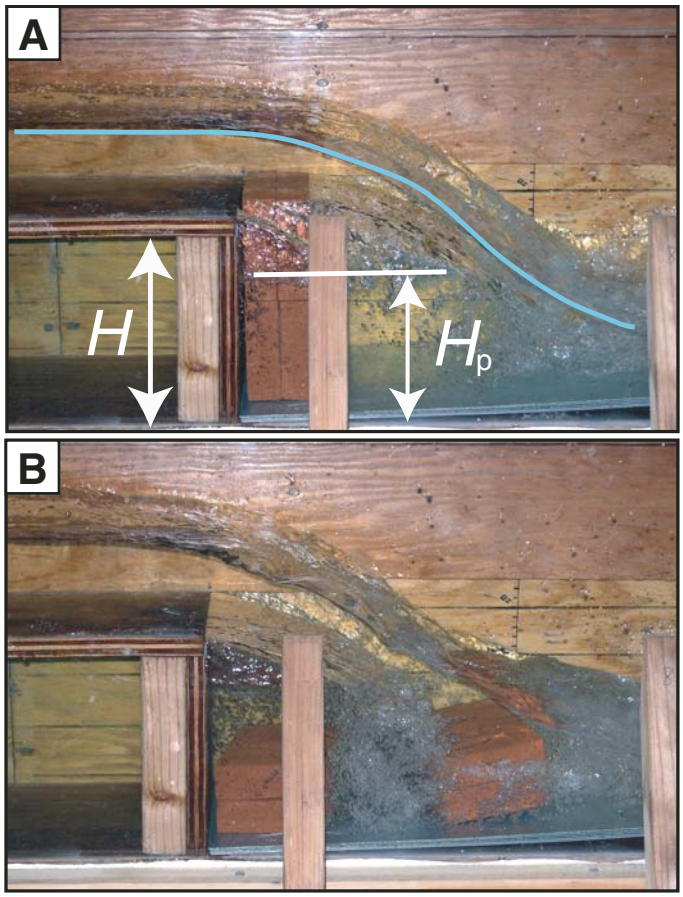

Figure 4. Photographs from experiments designed to test the toppling model. (A) Two blocks (L = 6.0 cm) stacked on top of one another in front of the backward-facing step before failure occurred. The step height (H = 19.2 cm) and plunge-pool height (H_p) are noted. The approximate location of the water surface is drawn as a blue line. (B) Two blocks after failure. The blocks failed together as a column, and the top block slid to the right upon impact. Note the sheet metal that the bricks were placed on to adjust θ and η.

large to induce toppling. For these experiments, the overflowing water did not appear as in other experiments, but instead was deflected upward and projected downstream upon impact with the protruding column, resulting in a smaller than expected plunge-pool depth (Table 1).

It is difficult to estimate the shear stress at a waterfall since the flow is accelerating over the lip. Instead, we calculated the shear stress from $\tau_T = \rho g h S$ and measurements of flow depth ~1 m upstream from the waterfall lip, where the flow was visually uniform, and estimated the shear stress at the lip using an acceleration factor formulated in the next section. The depth-averaged flow velocity (U) and the Froude number ($Fr = U/\sqrt{gh}$) were also measured ~1 m from the waterfall lip using $U = q/h$, where q is the discharge per unit width. Experiments were repeated three to five times to assess experimental and measurement error before changing the experimental conditions.

Acceleration at the Waterfall

Rouse (1936) and Hager (1983) showed that the depth-averaged flow velocity at a waterfall lip (U_o) can be related through use of an acceleration factor (α) to the bed shear stress (τ_T), Froude number (Fr), and depth-averaged flow velocity (U) upstream where the flow is steady, approximately uniform, and unaffected by the waterfall (which is typically a distance of two to four channel depths; Hager, 1983) as

$$\alpha \equiv \frac{U_o}{U} = \frac{0.4 + Fr^2}{Fr^2} \text{ for } Fr > 1, \quad (6A)$$

$$\alpha = \frac{1.4}{Fr^{2/3}} \text{ for } Fr < 1. \quad (6B)$$

By use of a spatially uniform friction coefficient, we can relate the shear stress at the waterfall (τ_o) to the shear stress upstream (e.g., following Stein and Julien, 1993; Flores-Cervantes et al., 2006; Haviv et al., 2006) as

$$\frac{\tau_o}{\tau_T} = \frac{\rho C_{f1} U_o^2}{\rho C_{f1} U^2} = \alpha^2, \quad (7)$$

where C_{f1} is a friction coefficient. Equation 7 implicitly assumes that drag due to the protrusion of bedrock columns into the flow does not affect the partitioning of stress upstream of the waterfall. By letting the flow velocity about the protruding portion of the column U_η follow a similar scaling, we can write

$$\frac{U_\eta}{U} = \frac{\sqrt{\tau_o / \rho C_{f2}}}{\sqrt{\tau_T / \rho C_{f1}}} = \alpha \sqrt{\frac{C_{f1}}{C_{f2}}}, \quad (8)$$

where $C_{f2} \le C_{f1}$ because U_η is averaged over a lower portion of the water column than U.

Experimental Results

The conditions needed to induce toppling in our flume experiments are shown in Table 1. In the experiments, flow depth upstream of the waterfall varied from $3 \le h \le 13$ cm and velocity varied from $0.8 \le U \le 2.7$ m/s. The flume-bed slope ranged from $0.0083 \le S \le 0.097$, and all runs had supercritical flow upstream of the waterfall with $1.14 \le Fr \le 3.48$. The angle of the brick column was varied independently of the flume-bed slope (Table 1). The plunge-pool depth ranged from H_p = 6 cm to fully submerged at H_p = 19 cm. In order to apply the model, the torque due to drag at the waterfall lip was calculated from Equations 2 and 8, where we assumed $C_{f2} = C_{f1}$ and $C_d = 1$ for simplicity.

Figure 5 shows the results of the measured torque balance at failure for each experiment without differentiation as to whether one or two bricks failed. The results are clustered with respect to gravitational torque, where the wider and taller columns at the time of failure required more torque to destabilize. Drag dominated over shear in all cases, which was intentionally designed into the experiments by letting $\eta > 0$. The data are more scattered for the widest bricks (L = 9.7 cm) because η/h was large and the flow and plunge pool were significantly affected by the column protrusion (as discussed in the Experimental Setup section). The model predictions (i.e., Equation 4 with FS = 1) match

TABLE 1. EXPERIMENTAL RESULTS

Exp. no.	S	tan θ	h (cm)	L (cm)	η (mm)	H_p (cm)	q (L/s)	U (m/s)	Fr	Toppled
1	0.008	–0.033	7.7	3.0	7.0	6.3	77	1.00	1.15	1
2	0.008	–0.033	6.9	3.0	7.0	16.0	66	0.96	1.17	2
3	0.008	–0.033	6.4	3.0	7.0	14.5	63	0.98	1.23	2
4	0.008	–0.033	6.7	3.0	7.0	15.0	64	0.95	1.18	2
5	0.008	–0.033	6.5	3.0	7.0	14.5	64	0.98	1.23	2
6	0.008	–0.054	8.0	3.0	7.0	7.1	81	1.01	1.14	1
7	0.008	–0.054	7.7	3.0	7.0	6.8	79	1.03	1.19	1
8	0.008	–0.054	7.5	3.0	7.0	6.3	77	1.02	1.19	1
9	0.008	–0.054	7.2	3.0	7.0	6.3	70	0.98	1.16	1
10	0.008	–0.054	7.8	3.0	7.0	6.3	79	1.02	1.16	1
11	0.008	–0.075	8.7	3.0	7.0	8.3	95	1.09	1.18	1
12	0.008	–0.075	8.2	3.0	7.0	7.3	87	1.06	1.19	1
13	0.008	–0.075	7.3	3.0	7.0	6.3	70	0.96	1.14	1
14	0.008	–0.075	7.7	3.0	7.0	6.8	81	1.05	1.21	1
15	0.008	–0.075	7.7	3.0	7.0	7.3	82	1.07	1.23	1
16	0.008	–0.013	6.4	3.0	7.0	14.0	61	0.96	1.21	2
17	0.008	–0.013	6.0	3.0	7.0	13.5	56	0.94	1.22	2
18	0.008	–0.013	6.0	3.0	7.0	13.5	56	0.94	1.22	2
19	0.008	–0.013	6.0	3.0	7.0	13.5	56	0.94	1.22	2
20	0.008	0.008	4.4	3.0	7.0	11.0	35	0.80	1.22	2
21	0.008	0.008	5.5	3.0	7.0	14.0	48	0.88	1.20	2
22	0.008	0.008	3.9	3.0	7.0	10.5	33	0.84	1.36	2
23	0.008	0.008	5.0	3.0	7.0	12.0	46	0.91	1.31	2
24	0.018	0.018	3.0	3.0	7.0	9.5	29	0.96	1.78	2
26	0.018	0.018	3.6	3.0	7.0	12.0	37	1.02	1.71	2
27	0.018	0.018	3.4	3.0	7.0	12.0	34	1.00	1.74	2
28	0.018	–0.003	5.5	3.0	7.0	13.5	56	1.02	1.39	2
29	0.018	–0.003	5.2	3.0	7.0	13.0	54	1.03	1.44	2
30	0.018	–0.003	5.5	3.0	7.0	14.5	56	1.02	1.39	2
31	0.018	–0.024	6.1	3.0	7.0	14.5	66	1.09	1.41	2
32	0.018	–0.024	6.0	3.0	7.0	14.5	63	1.04	1.36	2
33	0.018	–0.024	6.0	3.0	7.0	14.4	64	1.06	1.39	2
34	0.018	–0.045	6.5	3.0	7.0	5.8	73	1.12	1.41	1
35	0.018	–0.045	6.7	3.0	7.0	5.8	73	1.09	1.34	1
36	0.018	–0.045	6.2	3.0	7.0	5.6	68	1.09	1.40	1
37	0.018	–0.045	10.5	6.0	7.0	10.3	147	1.40	1.38	1
38	0.018	–0.045	10.5	6.0	7.0	19.0	146	1.39	1.37	2
39	0.018	–0.045	11.1	6.0	7.0	10.3	164	1.47	1.41	1
40	0.018	–0.045	10.5	6.0	7.0	10.3	151	1.44	1.41	1
41	0.018	–0.066	10.5	6.0	7.0	10.8	151	1.44	1.41	1
42	0.018	–0.066	10.7	6.0	7.0	12.3	157	1.47	1.43	1
43	0.018	–0.066	10.5	6.0	7.0	10.3	149	1.42	1.40	1
44	0.018	–0.066	7.8	3.0	7.0	7.3	91	1.17	1.34	1
45	0.018	–0.066	7.5	3.0	7.0	6.8	83	1.11	1.30	1
46	0.018	–0.066	7.0	3.0	7.0	6.8	79	1.13	1.37	1
47	0.018	–0.024	6.1	3.0	7.0	15.0	64	1.05	1.35	2
48	0.018	–0.024	6.1	3.0	7.0	15.0	64	1.05	1.35	2
49	0.018	–0.024	5.9	3.0	7.0	15.0	60	1.02	1.34	2
50	0.018	–0.024	6.0	3.0	7.0	15.5	63	1.04	1.36	2
51	0.018	–0.024	9.5	6.0	7.0	18.5	127	1.34	1.39	2
53	0.018	–0.024	9.0	6.0	7.0	18.0	112	1.24	1.32	2
54	0.018	–0.024	9.0	6.0	7.0	18.0	113	1.26	1.34	2
55	0.018	–0.024	9.0	6.0	7.0	18.0	112	1.24	1.32	2
56	0.018	–0.003	6.7	6.0	7.0	16.0	126	1.88	2.32	2
57	0.018	–0.003	6.7	6.0	7.0	15.5	74	1.11	1.37	2
58	0.018	–0.003	6.7	6.0	7.0	15.5	74	1.11	1.37	2
59	0.097	0.097	4.0	9.7	34.5	11.0	64	1.60	2.55	2
60	0.097	0.097	3.1	9.7	34.5	11.0	48	1.56	2.83	2
61	0.097	0.097	3.3	9.7	34.5	11.0	64	1.97	3.48	2
62	0.097	0.097	2.5	9.7	34.5	11.0	38	1.52	3.07	2
63	0.097	0.097	2.3	9.7	34.5	11.0	38	1.65	3.47	2
64	0.097	0.097	11.5	9.7	16.5	11.0	295	2.56	2.41	2
65	0.097	0.097	12.5	9.7	16.5	11.5	332	2.66	2.40	2
66	0.097	0.097	9.5	9.7	26.0	10.0	218	2.30	2.38	2
67	0.097	0.097	9.5	9.7	26.0	10.0	218	2.30	2.38	2
68	0.097	0.097	9.0	9.7	26.0	9.0	205	2.28	2.43	2
69	0.097	0.097	10.5	9.7	26.0	10.5	248	2.36	2.33	2
70	0.097	0.097	8.0	9.7	26.0	7.0	171	2.14	2.42	2
71	0.097	0.097	9.5	9.7	26.0	9.0	213	2.24	2.32	2

Note: The field "toppled" denotes the number of bricks that toppled during an experiment, where "2" indicates that both bricks toppled as a column. See text and notation list for definitions.

the experimental results well. In most cases, the sum of the torque due to shear, drag, and buoyancy at the point of toppling equaled the expected stabilizing torque due to gravity.

Figure 6 shows the experimental results and predictions for the relative stability of the top brick versus the entire column (i.e., Eq. 5 with $\gamma = 0.5$) for the case $L = 3$ cm. The results show two distinct regimes favoring either toppling of the entire column or the top brick, with the transition occurring at about tan θ = –0.03. As illustrated in the Torque-Balance Model section, in the absence of a differential buoyancy force (i.e., $H_p = 0$ or $H_p = H$), the transition would be expected at tan θ = 0. The finite plunge-pool depth, however, favors toppling of the entire column, which shifts the transition to negative brick angles. These experimental results match the predictions well, both in the magnitude of FS_γ/FS and in the relative stability of the column versus the top brick. Because the relative stability depends on the plunge-pool depth (H_p), the predicted values of FS_γ/FS were calculated using the average measured plunge-pool depth for each set of experiments.

FIELD APPLICATION

Equations 4 and 5 can be used to predict the geometry of upstream-propagating headwalls and the magnitude of flow necessary to induce toppling in natural systems. It is useful to explore the parameter space with respect to column aspect ratio (H/L) and tilt angle (θ) to describe the expected geometry of propagating waterfalls in fractured rock (Fig. 7). The aspect ratio $H/L = 0.5$ separates the fields of toppling from sliding assuming a friction angle of 45° along horizontal joint surfaces (Selby, 1993). The sliding regime will necessarily produce a more diffusive or stair-step headwall. Within the toppling regime, a block will fail due to gravity alone (in the absence of water flow) if it is tilted beyond a critical angle given by tan θ > L/H (i.e., where $T_g = 0$ in Eq. 2) (Fig. 7) (Goodman and Bray, 1977). For gravitationally stable blocks, positive tilt angles (tan θ > 0) always favor toppling of the entire column and therefore should preserve a steep headwall during upstream propagation. Steep headwalls can also persist at negative tilt angles, but this depends on the spacing of horizontal joints within a column (i.e., γ) and the relative height of the plunge pool (i.e., H_p/H), as described below.

By setting $FS_\gamma/FS = 1$, Equation 5 can be simplified to find the boundary between the vertical and stair-step headwall regimes as

$$\sin\theta = -\frac{\rho}{\rho_r}\frac{H_p}{H}\frac{L}{H}\left(\frac{1}{1-\gamma}\right). \qquad (9)$$

The largest difference in buoyancy between the entire column and any individual block occurs if the plunge-pool elevation is at the same level as the joint that defines the bottom of the block of interest (i.e., $H_p = H[1-\gamma]$), so that the entire top block is not submerged. Inserting this condition into Equation 9 results in the maximum (negative) angle possible for toppling of the entire column:

$$\sin\theta = -\frac{\rho}{\rho_r}\frac{L}{H}. \qquad (10)$$

Therefore, for $\sin\theta < -\frac{\rho}{\rho_r}\frac{L}{H}$, a headwall is predicted to form a stair-step pattern (Fig. 7). For $-\frac{\rho}{\rho_r}\frac{L}{H} < \sin\theta < 0$, either a stair-step pattern or a vertical headwall can result, and this depends on Equation 9.

Where toppling is likely to occur, Equation 4 can be used to predict the magnitude of flow necessary to induce failure. To illustrate this, we examine the deeply incised canyons with near-vertical, amphitheater headwalls that exist as tributary canyons to the Snake River Canyon in central Idaho (e.g., Malad Gorge, Blue Springs Canyon, and Box Canyon) (Fig. 1A). All of these canyons are thought to have formed by catastrophic paleofloods of various sources during the Quaternary that poured over the wall of the Snake River Canyon creating upstream-propagating waterfalls. Malad Gorge has three main canyon heads (e.g., Figs. 1B, 1C, and 1D) that were probably carved by large flood events of the Big and Little Wood Rivers (Kauffman et al., 2005). Blue Springs Canyon (Fig. 1E) was cut by the Eden Channel of the great Bonneville Flood, which catastrophically drained paleo–Lake Bonneville at ca. 15 ka (Malde, 1968; O'Connor, 1993). Box Canyon (Figs. 1F and 1G) was cut ca. 45 ka by a megaflood that probably initiated in the Wood or Lost River drainage basins (Lamb et al., 2008).

The Quaternary basalt that makes up the canyon walls ranges in age from ca. 80 ka to 400 ka (Tauxe et al., 2004; Kauffman et al., 2005; Aciego et al., 2007), is blocky and hard, and shows no visual evidence of significant chemical weathering or undercutting (Figs. 1C, 1D, and 1G). The headwalls of these canyons are on the order of 30–50 m high, and the basalt contains near-horizontal joints along bedding surfaces and near-vertical cooling joints, with spacings between joints of ~0.5 m (Figs. 1C, 1D, and 1G). Measurements of boulder sizes on the floor of Box Canyon, for example, yielded a median boulder size of 0.3 m (Lamb et al., 2008), which is consistent with our visual estimate of joint spacing. The landscape upstream

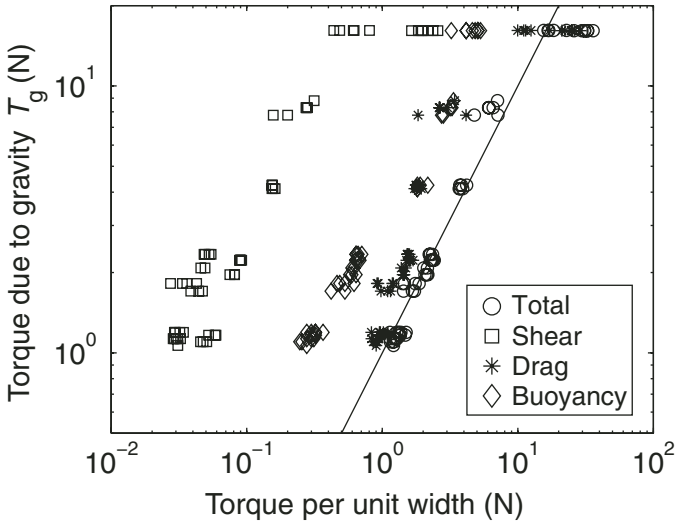

Figure 5. Experimental results and model predictions for the torque due to shear, drag, buoyancy, and the sum of all three vs. the torque due to gravity. The line indicates a 1:1 correlation corresponding to *FS* = 1 in Equation 4.

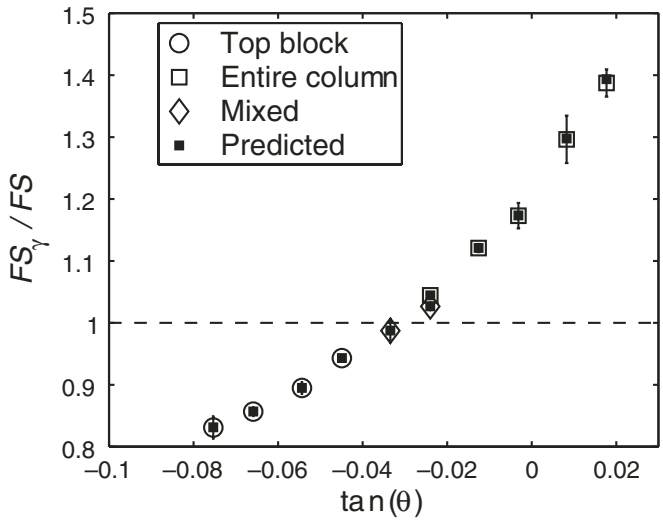

Figure 6. Experimental results (open markers) and model predictions (filled markers) for the relative stability of a stack of blocks. A column composed of two stacked blocks was used in the experiments. Where $FS_\gamma/FS > 1$, the model predicts that the entire column should fail before the top block. The small filled squares are model predictions (Eq. 5) using the values of plunge-pool depth (H_p) observed in the experiments. The open markers represent the mean and the error bars represent the standard deviation of 3–5 runs with the same experimental conditions (Table 1). Error bars not shown are smaller than the marker size. The diamond markers are for cases where the results were mixed between failure of the top block and the entire column. Only the results for *L* = 3.0 cm are shown; the results for *L* = 6.0 cm yielded similar trends (Table 1), and cases with *L* = 9.7 cm could not be explored for tan θ < 0 due to flume constraints.

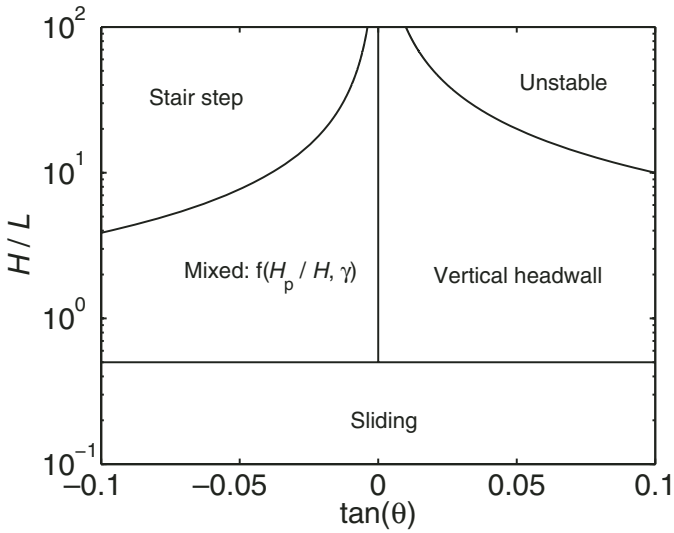

Figure 7. Stability fields for a column of rock composed of a stack of blocks. The region marked "Unstable" is gravitationally unstable in the absence of water flow. A vertical headwall is predicted to persist during upstream propagation in the field marked "Vertical headwall." Alternatively, the headwall is predicted to diffuse or form a stair-step pattern in the regime marked "Stair step." In between, the field marked "Mixed" is where the relative stability depends on the plunge-pool height and the horizontal joint spacing (i.e., Eq. 9). For blocks with small aspect ratios ($H/L < 0.5$), sliding is probably more likely than toppling. Note that for this range in slopes, tan θ ≈ sin θ.

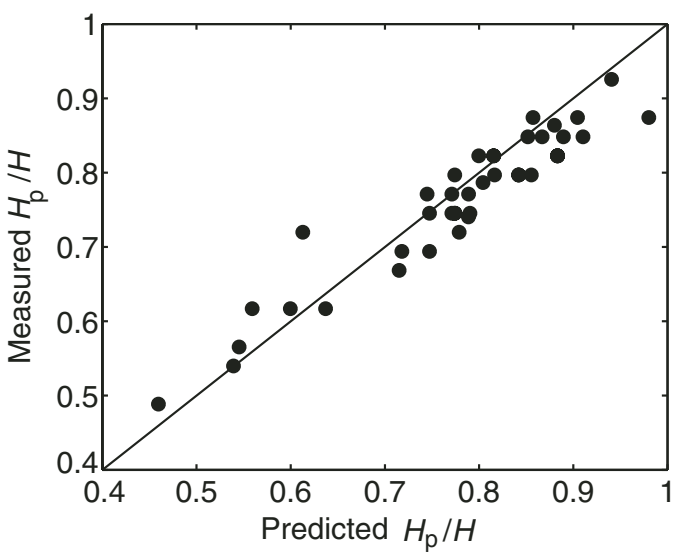

Figure 8. Measured vs. predicted (Eq. 13) plunge-pool heights normalized by the column height. The results for L = 9.7 cm are not shown, since large η/h disturbed the formation of the plunge pool (see text for details). The line represents a 1:1 correlation.

of these canyon heads is relatively flat, but it does dip toward the canyons with a slope of ~1% (Fig. 1A). Because bedding planes are probably on average parallel to the land surface, and near-vertical joints are perpendicular to the land surface (Budkewitsch and Robin, 1994), Equation 5 predicts, given sufficient flow, that rotational failure should occur at the base of the columns, preserving their steep headwalls (i.e., tan θ = S > 0; Fig. 7). Therefore, Equation 4 can be used to estimate the flow conditions needed to cause toppling failure of rock columns that extend the total relief of the canyon headwalls.

First, it is useful to rewrite the flow velocity in Equation 4 in terms of total bed stress (using Eq. 8) and to assume steady and uniform flow (i.e., $\tau_r = \rho g h S$) upstream from the headwall. This modification results in

$$FS = \frac{\frac{\rho_r}{\rho}\cos\theta\left(1-\frac{HS}{L}\right)-\frac{H_p}{H}}{\frac{2\alpha^2 hS}{L}\left(1+\frac{1}{2}\frac{C_d}{C_{f2}}\frac{\eta}{L}\right)}, \qquad (11)$$

where α can be simplified to

$$\alpha = 0.4\frac{C_{f1}}{S}+1 \text{ for } Fr > 1 \text{ and} \qquad (12A)$$

$$\alpha = 1.4\left(\frac{C_{f1}}{S}\right)^{1/3} \text{ for } Fr < 1. \qquad (12B)$$

All variables in Equations 11 and 12 can be estimated or measured from the topography and geometry of the canyons except the plunge-pool depth. The depth of water behind a waterfall at a vertical drop can be calculated following theory for a two-dimensional (2-D) plane jet impinging on a horizontal plane at steady state (Leske, 1963; Vischer and Hager, 1995; Chanson, 2002):

$$\frac{H_p}{h} = \left(1+2(1-\cos\delta)Fr^2\right)^{1/2}, \qquad (13)$$

where $\cos\delta = \left[\frac{2+Fr_o^2}{2+Fr_o^2+2\alpha^{2/3}H/h}\right]^{1/2}$

is the angle of the jet relative to horizontal, and $Fr_o^2 = \alpha^3 Fr^2 = \alpha^3 S / C_{f1}$ is the Froude number at the overflow point squared. Equation 13 provides a good prediction of the observed pool heights in our flume experiments (Fig. 8), except for the cases with large η/h (i.e., L = 9.7 cm), where plunge-pool development was disturbed.

Equations 11–13 reveal that the flood stage necessary to produce toppling failure (i.e., FS = 1) normalized by the column width (h/L) is a function of six dimensionless parameters: H/L, S, η/L, ρ_r/ρ, C_{f1}, and C_d/C_{f2}. For the basalt columns of interest, we set ρ_r/ρ = 2.8, $C_{f1} = C_{f2}$

$= 5 \times 10^{-3}$ (corresponding to typical conditions of a gravel-bed river [e.g., Parker, 1991], and $C_d = 1$. Although the rock columns in Idaho do not abruptly protrude into the flow as in our flume experiments, the roughness of their top surfaces probably results in wake formation and therefore a component of form drag (Batchelor, 1967). Form drag is taken into account in the model by setting $\eta/L = 0.1$, which is based on our observations in Idaho of roughness length scales on the order of 0.05 m and column widths of ~0.5 m. With these assumptions, h/L is now only a function of the aspect ratio of the columns (H/L) and the average slope of the land surface (S).

Equations 11–13 were solved for a range of column aspect ratios and slopes. Since h appears in both Equations 11 and 13, a numerical iteration was used to solve for h. As shown in Figure 9, larger aspect ratios and steeper slopes require less flow to induce toppling. For a range in column widths ($0.5 < L < 1$ m) and conditions typical of Box Canyon ($H = 35$ m and tan $\theta = 0.009$; Figs. 1A, 1F, and 1G), the calculated plunge-pool depths at the threshold of toppling range from 3 to 9 m, and the calculated flow depths upstream of the waterfall are $1.6 < h < 5.6$ m. This range is consistent with independent estimates of flow depth during canyon formation ($h > 3$ m) based on a survey of channel form upstream of the canyon head and incipient motion considerations for boulders within the canyon (Lamb et al., 2008). Thus, it seems that the flood flows at Box Canyon would have been competent to induce toppling and preserve a steep headwall, as well as transport collapsed boulders out of the canyon (Lamb et al., 2008). This necessary flood stage (Fig. 9) also seems reasonable for Malad Gorge and Blue Lakes Canyon given the magnitude of paleoflood events that have occurred there (Kauffman et al., 2005; O'Connor, 1993).

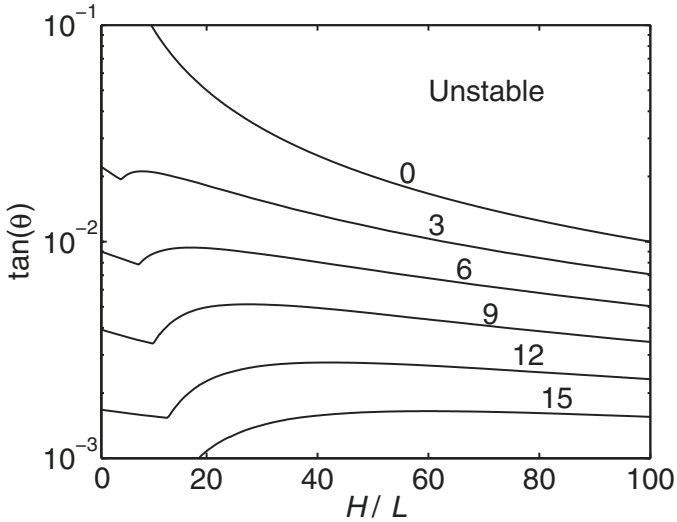

Figure 9. Contours of flow depth normalized by column width (h/L) at the threshold of rotational failure predicted by Equations 11–13 as a function of column tilt angle (tan θ) and column aspect ratio (H/L). To make model predictions, several assumptions typical of field conditions were used (as described in the text). Note that zero flow is needed to induce toppling for large tilt angles and large aspect ratios since these columns are gravitationally unstable. The kink in the contours at small H/L occurs where the columns are predicted to be fully submerged (i.e., $H_p = H$).

DISCUSSION

Interlocking

Our model and flume experiments of headwall retreat by toppling are for simple joint patterns that probably do not translate to all cases in nature. For example, within a column of rock at a headwall, some blocks might extend between otherwise free-standing columns or interlock with neighboring columns, and this may induce a yield strength that must be overcome for failure to occur. This could impact the predictions of flow needed to induce toppling and the morphology of the headwall (i.e., Eqs. 4 and 5). If yield strength varies with column height, then it is possible that a given block might fail before the entire column, even with a positive tilt angle. This appears to be the case for Apsley Gorge, Australia, where subvertical joints in metasedimentary rocks control the morphology of the headwall there (Weissel and Seidl, 1997). Although dominant joints dip in the downstream direction, the connectivity of joints apparently is not sufficient to create a vertical or overhanging headwall. Instead, toppling of blocks and overhangs occur at a local scale, whereas overall, the headwall is convex in profile (Weissel and Seidl, 1997). On the other hand, jointing appears to be pervasive enough in the basalt walls of the Idaho canyons that some vertical joints connect between stacked lava flows and outline free-standing columns of rock (Figs. 1C, 1D, and 1G).

Quantitative assessments of the strength of interlocking along vertical joints are difficult (Whipple et al., 2000). Unlike horizontal joint surfaces, where resistance to sliding can be calculated from the product of a friction angle and the weight of the overlying rock column (Terzaghi, 1962; Hancock et al., 1998), there is not a characteristic normal stress acting on vertical joints. Instead, the yield strength (if it exists) must be due to a sum of interlocked roughness elements within a joint plane, each of which has highly variable directions and magnitudes of local stress. The yield strength of interlocked columns probably depends on the roughness of joint surfaces, bedrock type, rock strength, degree of weathering, and fracture geometries. There is a clear need for future work to measure the yield strength of bedrock joints at field scale.

Pore Pressure

In addition to the forces already discussed, pore pressure might also be important for causing failure of a rock column. Pore pressure might be induced at a waterfall headwall due to infiltration and groundwater flow toward the headwall. A differential pore-water height across a column of rock would produce a force and a torque on the column, and if this is significant, it could induce toppling. This necessarily makes our factor of safety analysis conservative because it does not include pore-pressure gradients. Like buoyancy, torque caused by pore fluids should also favor toppling of the entire column over any individual block higher up in the column because hydrostatic water pressure scales linearly with water depth.

To first order, pore-pressure gradients can be estimated by assuming one-dimensional, steady-state Darcy flow within an unconfined aquifer (i.e., the Dupuit approximation; Freeze and Cherry, 1979),

$$q_p = -Kh_p \frac{dh_p}{dx}, \quad (14)$$

where q_p is the volumetric groundwater discharge (per unit width), K is the horizontal hydraulic conductivity, and h_p is the elevation of groundwater within the pore spaces as a function of horizontal distance (x). If we let h_p be the elevation of pore water within a vertical joint immediately before the waterfall and neglect the plunge-pool height, then

$\frac{dh_p}{dx} \approx -\frac{h_p}{L}$, and Equation 14 can be rewritten as

$$h_p = \sqrt{LD_i \frac{V_i}{K}}, \quad (15)$$

where $V_i = q_p/D_i$ is the steady-state infiltration rate, and D_i is the surface area per unit width over which infiltration occurs. Thus, pore pressure should be important for large infiltration rates, large infiltration distances, and small horizontal hydraulic conductivity.

Our small-scale experiments were intentionally designed to limit pore-pressure effects by making D_i small (i.e., only one vertical crack). This was done because V_i/K was large in our experiments due to the relatively large ratio of vertical joint spacing to column width, and K was small because we lacked joint planes parallel to the downstream direction of the flume. These effects were due to the small scale of our experiments and are probably not representative of the canyons of the Snake River Plain. For example, horizontal conductivity is large in the Snake River Plain owing to rubble zones, fissures, fractures, and lava tubes (Knutson et al., 1992), and average values of K are ~5 × 10^{-3} m/s, with maximum values as high as $K = 1 \times 10^{-2}$ m/s (Ackerman, 1991; Malde, 1991; Welhan and Reed, 1997). The headwall of Box Canyon, for example, is the site of one of the largest springs in the United States, with a discharge of ~9.5 m^3/s (Fig. 1B). Pond tests in the eastern Snake River Plain indicate average infiltration rates over several days of ~5 × 10^{-7} m/s; peak rates in the first several hours of each test were ~1 × 10^{-6} m/s (Faybishenko et al., 2000; Unger et al., 2004). Thus, for the Snake River Plain, $V_i/K \approx 10^{-4}$. Using this value and setting the column width to $L = 1$ m in Equation 15, the differential pore fluid height is calculated not to exceed $h_p = 1$ m, even if infiltration took place over a distance of $D_i = 10$ km upstream of the headwall. This suggests that differential pressure caused by pore fluid is probably not important in inducing toppling for the canyons of the Snake River Plain since the pore-fluid heights are small compared to both the column heights (H) and plunge-pool depths (H_p). This, however, might not be the case in other locations, especially where V_i/K is large.

Lateral Focusing of Flow

One of the limitations of our model is that both Equations 4 and 5 were formulated in terms of a unit channel width and neglect lateral changes in the flow. Spatial acceleration in flow might be important for the canyons of the Snake River Plain where unconfined flood water poured over the wall of the Snake River Canyon. In this case, the low pressure associated with overflow at the canyon head might have caused flow to focus toward the canyon head, resulting in faster flow there, and an increase in the rate of toppling and canyon-head retreat (e.g., by increasing α and H_p in Equation 4). This also makes our estimates of flow discharge needed to cause toppling conservative. Feedback between flow focusing and canyon-head retreat might explain why these flood events resulted in the formation of tributary canyons rather than broad escarpments. Furthermore, this mechanism might also explain the amphitheater planform of these canyon headwalls, such that toppling was more likely at the center of the headwall due to flow focusing, whereas the edges of the headwall were at or near the threshold of toppling. These three-dimensional effects need to be explored in future experimental and numerical model studies.

Implications for Mars

The surface of Mars has abundant canyons with steep amphitheater-shaped headwalls and knickpoints similar to those described here (e.g., Baker, 1982). Although these features are often attributed to seepage erosion (e.g., Baker, 1990; Malin and Carr, 1999; Harrison and Grimm, 2005; Luo and Howard, 2008), recent work suggests that waterfall erosion might be a more plausible mechanism, especially in hard rock (Craddock and Howard, 2002; Howard et al., 2005; Lamb et al., 2006, 2007, 2008). This is supported by the observation that many Martian valleys with steep headwalls have shallow tributaries upslope, suggesting that overspill occurred in the past (Irwin et al., 2004; Crown et al., 2005). Retreating waterfalls might have been initiated by flood water breaching the rim of an impact crater (e.g., Irwin and Howard, 2002; Howard et al., 2005) or the rim of a preexisting river canyon (as in Idaho; Fig. 1). For example, the 900-km-long Ma'adim Vallis was probably carved by catastrophic overflow of a highland lake resulting in a 300-m-high knickpoint in the main channel and hanging tributary canyons (Irwin et al., 2002, 2004). As another example, Williams and Malin (2004) described a 100-m-high near-vertical headwall of a channel within Kasei Valles that appears to represent a relict retreating waterfall. We hypothesize that the abundance of amphitheater-headed canyons and steep knickpoints on Mars might reflect a well-jointed lithology (e.g., columnar basalt), which is susceptible to toppling failure (and flood events sufficient to induce failure and transport collapsed material) rather than seepage erosion. Images of the surface of Mars have revealed layered material in canyon walls, and spectral data suggest that some of this is olivine-rich basalt (Bandfield et al., 2000; Christensen et al., 2003; Hamilton and Christensen, 2005). If our hypothesis is correct and fracture patterns can be observed or estimated, Equation 4 and Figure 9 can be used to calculate the flow required to cause toppling failure at the headwalls of Martian canyons. Because Equation 4 is based on a ratio of torques, the effects of lower Martian gravity are implicitly accounted for in the model.

CONCLUSIONS

We hypothesize that waterfalls can persist during upstream headwall retreat in the absence of undercutting due to toppling in well-jointed bedrock. A torque-balance model indicates that a column of rock at a waterfall is generally less stable than any given block that comprises it because of buoyancy produced by the plunge pool at the foot of the waterfall, a downstream tilt of the rock column, or both. The model provides good predictions of the flow needed to induce toppling and the resulting morphology of the headwalls in flume experiments and the amphitheater-headed canyons of the Snake River Plain, Idaho, that were carved by large-scale floods. This suggests that erosion of bedrock canyons by waterfall retreat can be rapid where bedrock is well jointed and flow is sufficient to topple rock columns and excavate the collapsed material. Where block toppling can explain the origin of steep waterfalls and amphitheater-headed canyons on Earth and Mars, the torque-balance model can be used to constrain the minimum discharge of water needed to carve these features. Overall, our work adds to the growing recognition that bedrock fracture geometry can play a fundamental role in knickpoint morphology and retreat rate, and therefore it needs to be incorporated into landscape evolution models.

ACKNOWLEDGMENTS

This work benefited from discussions with Leonard Sklar, Michael Manga, Christian Braudrick, and Peter Nelson. We thank Jeff Prancevic and John Potter for assistance with the experiments. We also thank

Joel Johnson, Les Hasbargen, and Carrie Jennings for helpful and constructive reviews that improved this paper. Support was provided by the U.S. Geological Survey, the National Center for Earth Surface Dynamics, and the National Astrobiology Institute (University of California BioMars program).

APPENDIX 1. NOTATION

C_d—Drag coefficient
C_{f1}—Friction coefficient for the depth-averaged flow
C_{f2}—Friction coefficient for the flow U_η
D_i—Infiltration distance
F_b—Buoyancy force
F_d—Drag force
F_g—Gravity force
F_s—Shear force
FS—Factor of safety
Fr—Froude number upstream from the overfall
Fr_o—Froude number at the overfall
g—Acceleration due to gravity
h—Flow depth upstream of the waterfall
h_p—Pore-water height
H—Total rock column height
H_γ—Block height
H_p—Plunge-pool depth
K—Hydraulic conductivity
L—Rock column length
q—Flow discharge per unit width
q_p—Groundwater discharge per unit width
S—Channel-bed slope
T_b—Torque due to buoyancy
T_d—Torque due to drag
T_g—Torque due to gravity
T_s—Torque due to shear
U—Depth-averaged flow velocity upstream of the waterfall
U_o—Depth-averaged flow velocity at the overfall
U_η—Flow velocity averaged over the protrusion distance η
V_i—Infiltration rate
α—Acceleration factor
β—Angle from horizontal of the water surface upstream headwall
δ—Jet impingement angle
γ—Ratio of block height to column height
η—Protrusion length scale
ρ—Density of the fluid
ρ_r—Density of the rock
θ—Angle of the rock column from horizontal
τ_o—Bed stress at the overfall
τ_η—Bed stress upstream from the overfall

REFERENCES CITED

Aciego, S.M., DePaolo, D.J., Kennedy, B.M., Lamb, M.P., Sims, K., and Dietrich, W.E., 2007, Combining [^{3}He] cosmogenic dating with U-Th/He eruption ages using olivine in basalt: Earth and Planetary Science Letters, v. 9, p. 288–302, doi: 10.1016/j.epsl.2006.11.03.

Ackerman, D.J., 1991, Transmissivity of the Snake River Plain Aquifer at the Idaho National Engineering Laboratory, Idaho: U.S. Geological Survey Water-Resources Investigation Report 91–4085, 35 p.

Alonso, C.V., Bennett, S.J., and Stein, O.R., 2002, Predicting headcut erosion and migration in concentrated flows typical of upland areas: Water Resources Research, v. 38, no. 12, 15 p., doi: 10.1029/2001WR001173.

Annandale, G.W., 1995, Erodibility: Journal of Hydraulic Research, v. 33, no. 4, p. 471–494.

Aydin, A., and DeGraff, J.M., 1988, Evolution of polygonal fracture patterns in lava flows: Nature, v. 239, p. 471–476.

Baker, V.R., 1973, Paleohydrology and Sedimentology of the Lake Missoula Flooding in Eastern Washington: Geological Society of America Special Paper 144, 79 p.

Baker, V.R., 1982, The Channels of Mars: Austin, University of Texas Press, 198 p.

Baker, V.R., 1990, Spring sapping and valley network development, with case studies by R.C. Kochel, V.R. Baker, J.E. Laity, and A.D. Howard, *in* Higgins, C.G., and Coates, D.R., eds., Groundwater Geomorphology; The Role of Subsurface Water in Earth-Surface Processes and Landforms: Geological Society of America Special Paper 252, p. 235–265.

Bandfield, J.L., Hamilton, V.E., and Christensen, P.R., 2000, A global view of Martian surface compositions from MGS-TES: Science, v. 287, no. 5458, p. 1626–1630, doi: 10.1126/science.287.5458.1626.

Batchelor, G.K., 1967, An Introduction to Fluid Mechanics: London, Cambridge University Press, 615 p.

Bennett, S.J., 1999, Effect of slope on the growth and migration of headcuts in rills: Geomorphology, v. 30, no. 3, p. 273–290, doi: 10.1016/S0169-555X(99)00035-5.

Berlin, M. M., and Anderson, R. S., 2007, Modeling knickpoint retreat on the Roan Plateau, western Colorado: Journal of Geophysical Research, v. 112, F03S06, doi: 10.1029/2006JF000553.

Bishop, P., Hoey, T.B., Jansen, J.D., and Artza, I.L., 2005, Knickpoint recession rate and catchment area: The case of uplifted rivers in eastern Scotland: Earth Surface Processes and Landforms, v. 30, no. 6, p. 767–778, doi: 10.1002/esp.1191.

Bretz, J.H., 1923, The channeled scabland of the Columbia Plateau: The Journal of Geology, v. 31, p. 617–649.

Budkewitsch, P., and Robin, P.Y., 1994, Modeling the evolution of columnar joints: Journal of Volcanology and Geothermal Research, v. 59, p. 219–239, doi: 10.1016/0377-0273(94)90092-2.

Chanson, H., 2002, The Hydraulics of Stepped Chutes and Spillways: Lisse, Swets & Zeitlinger B.V., 384 p.

Chatanantavet, P., and Parker, G., 2005, Modeling the bedrock evolution of western Kaua'i, Hawai'i, by a physically-based incision model based on abrasion, *in* Parker, G., and Garcia, M., eds., River, Coastal, and Estuarine Morphodynamics: International Association of Hydraulic Engineering and Research Symposium: London, Taylor and Francis, p. 99–110.

Christensen, P.R., Bandfield, J.L., Bell, J.F., Gorelick, N., Hamilton, V.E., Ivanov, A., Jakosky, B.M., Kieffer, H.H., Lane, M.D., Malin, M.C., McConnochie, T., McEwen, A.S., McSween, H.Y., Mehall, G.L., Moersch, J.E., Nealson, K.H., Rice, J.W., Richardson, M.I., Ruff, S.W., Smith, M.D., Titus, T.N., and Wyatt, M.B., 2003, Morphology and composition of the surface of Mars: Mars Odyssey THEMIS results: Science, v. 300, no. 5628, p. 2056–2061, doi: 10.1126/science.1080885.

Coleman, S.E., Melville, B.W., and Gore, L., 2003, Fluvial entrainment of protruding fractured rock: Journal of Hydraulic Engineering, v. 129, no. 11, p. 872–884, doi: 10.1061/(ASCE)0733-9429(2003)129:11(872).

Craddock, R.A., and Howard, A.D., 2002, The case for rainfall on a warm, wet early Mars: Journal of Geophysical Research–Planets, v. 107, no. E11, doi: 10.1029/2001JE001505.

Crosby, B.T., Whipple, K.X., Gasparini, N.M., and Wobus, C.W., 2007, Formation of fluvial hanging valleys: Theory and simulation: Journal of Geophysical Research–Earth Surface, v. 112, no. F3, doi: 10.1029/2006JF000566.

Crown, D.A., Bleamaster, L.F., and Mest, S.C., 2005, Styles and timing of volatile-driven activity in the eastern Hellas region of Mars: Journal of Geophysical Research–Planets, v. 110, no. E12, doi: 10.1029/2005JE002496.

Dunne, T., 1990, Hydrology, mechanics, and geomorphic implications of erosion by subsurface flow, *in* Higgins, C.G., and Coates, D.R., eds., Groundwater Geomorphology; The Role of Subsurface Water in Earth-Surface Processes and Landforms: Geological Society of America Special Paper 252, p. 1–28.

Faybishenko, B., Doughty, C., Steiger, M., Long, J.C.S., Wood, T.R., Jacobsen, J.S., Lore, J., and Zawislanski, P.T., 2000, Conceptual model of the geometry and physics of water flow in a fractured basalt vadose zone: Water Resources Research, v. 36, no. 12, p. 3499–3520, doi: 10.1029/2000WR900144.

Flores-Cervantes, J.H., Istanbulluoglu, E., and Bras, R.L., 2006, Development of gullies on the landscape: A model of headcut retreat resulting from plunge pool erosion: Journal of Geophysical Research–Earth Surface, v. 111, no. F1, doi: 10.1029/2004JF000226.

Frankel, K.L., Pazzaglia, F.J., and Vaughn, J.D., 2007, Knickpoint evolution in a vertically bedded substrate, upstream-dipping terraces, and Atlantic slope bedrock channels: Geological Society of America Bulletin, v. 119, no. 3/4, p. 476–486, doi: 10.1130/B25965.1.

Freeze, R.A., and Cherry, J.A., 1979, Groundwater: Englewood Cliffs, New Jersey, Prentice-Hall, Inc., 604 p.

Gardner, T.W., 1983, Experimental-study of knickpoint and longitudinal profile evolution in cohesive, homogeneous material: Geological Society of America Bulletin, v. 94, no. 5, p. 664–672, doi: 10.1130/0016-7606(1983)94<664:ESOKAL>2.0.CO;2.

Gasparini, N.M., Whipple, K.X., and Bras, R.L., 2007, Predictions of steady state and transient landscape morphology using sediment-flux–dependent river incision models: Journal of Geophysical Research–Earth Surface, v. 112, no. F3, doi: 10.1029/2006JF000567.

Gilbert, G.K., 1907, The Rate of Recession of Niagara Falls: U.S. Geological Survey Bulletin 306, 25 p.

Goodman, N.M., and Bray, J.W., 1977, Toppling of Rock Slopes, *in* Rock Engineering for Foundations and Slopes: New York, American Society of Civil Engineers, p. 201–234.

Hager, W.H., 1983, Hydraulics of plane free overfall: Journal of Hydraulic Engineering, v. 109, no. 12, p. 1683–1697.

Hamilton, V.E., and Christensen, P.R., 2005, Evidence for extensive, olivine-rich bedrock on Mars: Geology, v. 33, no. 6, p. 433–436, doi: 10.1130/G21258.1.

Hancock, G.S., Anderson, R.S., and Whipple, K.X., 1998, Beyond power: Bedrock river incision process and form, *in* Tinkler, K.J., and Wohl, E.E., eds., Rivers Over Rock: Washington, D.C., American Geophysical Union, p. 35–60.

Harrison, K.P., and Grimm, R.E., 2005, Groundwater-controlled valley networks and the decline of surface runoff on early Mars: Journal of Geophysical Research–Planets, v. 110, no. E12, S16, doi: 10.1029/2005JE002455.

Haviv, I., Enzel, Y., Whipple, K.X., Zilberman, E., Stone, J., Matmon, A., and Fifield, L.K., 2006, Amplified erosion above waterfalls and oversteepened bedrock reaches: Journal of Geophysical Research, v. 111, F040004, doi: 10.1029/2006JF000461.

Holland, W.N., and Pickup, G., 1976, Flume study of knickpoint development in stratified sediment: Geological Society of America Bulletin, v. 87, no. 1, p. 76–82, doi: 10.1130/0016-7606(1976)87<76:FSOKDI>2.0.CO;2.

Howard, A.D., and McLane, C.F., 1988, Erosion of cohesionless sediment by groundwater seepage: Water Resources Research, v. 24, no. 10, p. 1659–1674, doi: 10.1029/WR024i010p01659.

Howard, A.D., Dietrich, W.E., and Seidl, M.A., 1994, Modelling fluvial erosion on regional and continental scales: Journal of Geophysical Research–Solid Earth, v. 99, p. 13,971–13,986, doi: 10.1029/94JB00744.

Howard, A.D., Moore, J.M., and Irwin, R.P., 2005, An intense terminal epoch of widespread fluvial activity on early Mars: 1. Valley network incision and associated deposits: Journal of Geophysical Research–Planets, v. 110, no. E12, doi: 10.1029/2005JE002459.

Irwin, R.P., and Howard, A.D., 2002, Drainage basin evolution in Noachian Terra Cimmeria, Mars: Journal of Geophysical Research–Planets, v. 107, no. E7, doi: 10.1029/2001JE001818.

Irwin, R.P., Maxwell, T.A., Howard, A.D., Craddock, R.A., and Leverington, D.W., 2002, A large paleolake basin at the head of Ma'adim Vallis, Mars: Science, v. 296, no. 5576, p. 2209–2212, doi: 10.1126/science.1071143.

Irwin, R.P., Howard, A.D., and Maxwell, T.A., 2004, Geomorphology of Ma'adim Vallis, Mars, and associated paleolake basins: Journal of Geophysical Research–Planets, v. 109, no. E12, doi: 10.1029/2004JE002287.

Kauffman, J.D., Otherberg, K.L., Gillerman, V.S., and Garwood, D.L., 2005, Geologic map of the Twin Falls 30 × 60 minute quadrangle, Idaho: Moscow, Idaho, Idaho Geological Survey, scale 1:100,000.

Knutson, C., McCormick, K.A., Crocker, J.C., Glenn, M.A., and Fishel, M.L., 1992, 3D RWMC Vadose Zone Modeling: EG&G Internal Report EGG-WM-8949, 126 p.

Kochel, R.C., Howard, A.D., and McLane, C.F., 1985, Channel networks developed by groundwater sapping in fine-grained sediments; analogs to some Martian valleys, *in* Woldenberg, M., ed., Models in Geomorpholgy: London, Allen and Unwin, p. 313–341.

Laity, J.E., and Malin, M.C., 1985, Sapping processes and the development of theater-headed valley networks on the Colorado Plateau: Geological Society of America Bulletin, v. 96, p. 203–217, doi: 10.1130/0016-7606(1985)96<203:SPATDO>2.0.CO;2.

Lamb, M.P., Howard, A.D., Johnson, J., Whipple, K.X., Dietrich, W.E., and Perron, J.T., 2006, Can springs cut canyons into rock?: Journal of Geophysical Research–Planets, v. 111, E07002, doi: 10.1029/2005JE002663.

Lamb, M.P., Howard, A.D., Dietrich, W.E., and Perron, J.T., 2007, Formation of amphitheater-headed valleys by waterfall erosion after large-scale slumping on Hawai'i: Geological Society of America Bulletin, v. 119, p. 805–822, doi: 10.1130/B25986.1.

Lamb, M.P., Dietrich, W.E., Aciego, S.M., DePaolo, D., and Manga, M., 2008, Formation of Box Canyon, Idaho, by megaflood: Implications for seepage erosion on Earth and Mars: Science, v. 320, p. 1067, doi: 10.1126/science.1156630.

Leske, 1963, Die Umlenkung eines frei herabfallenden, ebenen Strahls an einer horizontalen Sohle: Wissenschaftliche Zeitschrift TU Dresden, v. 12, no. 6, p. 1749–1765.

Lobkovsky, A.E., Smith, B.E., Kudrolli, A., Mohrig, D.C., and Rothman, D.H., 2007, Erosive dynamics of channels incised by subsurface water flow: Journal of Geophysical Research–Earth Surface, v. 112, no. F3, 10 p, doi: 10.1029/2006JF000517.

Luo, W., and Howard, A.D., 2008, Computer simulation of the role of groundwater seepage in forming Martian valley networks: Journal of Geophysical Research, v. 113, E05002, doi: 10.1029/2007JE002981.

Malde, H.E., 1968, The Catastrophic Late Pleistocene Bonneville Flood in the Snake River Plain, Idaho: U.S. Geological Survey Professional Paper 596, p. 1–52.

Malde, H.E., 1991, Quaternary geology and structural history of the Snake River Plain, Idaho and Oregon, *in* Morrison, R.B., ed., Quaternary Nonglacial Geology; Conterminous U.S.: Boulder, Colorado, Geological Society of America, The Geology of North America, v. K–2 p. 617–628.

Malin, M.C., and Carr, M.H., 1999, Groundwater formation of Martian valleys: Nature, v. 397, no. 6720, p. 589–591, doi: 10.1038/17551.

Miller, J.R., 1991, The influence of bedrock geology on knickpoint development and channel-bed degradation along downcutting streams in south-central Indiana: The Journal of Geology, v. 99, p. 591–605.

Miller, J.R., and Dunne, T., 1996, Topographic perturbations of regional stresses and consequent bedrock fracturing: Journal of Geophysical Research, v. 101, no. B11, p. 25,523–25,536, doi: 10.1029/96JB02531.

O'Connor, J.E., 1993, Hydrology, Hydraulics and Geomorphology of the Bonneville Flood: Geological Society of America Special Paper 274, 90 p.

Parker, G., 1991, Selective sorting and abrasion of river gravel. II: Applications: Journal of Hydraulic Engineering, v. 117, no. 2, p. 150–171.

Pederson, D.T., 2001, Stream piracy revisited: A groundwater sapping solution: GSA Today, v. 11, no. 9, p. 4–10, doi: 10.1130/1052-5173(2001)011<0004:SPRAGS>2.0.CO;2.

Philbrick, S.S., 1970, Horizontal configuration and the rate of erosion of Niagara Falls: Geological Society of America Bulletin, v. 81, p. 3723–3732, doi: 10.1130/0016-7606(1970)81[3723:HCATRO]2.0.CO;2.

Philbrick, S.S., 1974, What future for Niagara Falls?: Geological Society of America Bulletin, v. 85, no. 1, p. 91–98, doi: 10.1130/0016-7606(1974)85<91:WFFNF>2.0.CO;2.

Rouse, H., 1936, Discharge characteristics of the free overfall: Civil Engineering, v. 7, p. 518.

Seidl, M.A., Dietrich, W.E., and Kirchner, J.W., 1994, Longitudinal profile development into bedrock: An analysis of Hawaiian channels: The Journal of Geology, v. 102, p. 457–474.

Seidl, M.A., Weissel, J.K., and Pratson, L.F., 1996, The kinematics and pattern of escarpment retreat across the rifted continental margin of SE Australia: Basin Research, v. 8, no. 3, p. 301–316, doi: 10.1046/j.1365-2117.1996.00266.x.

Seidl, M.A., Finkel, R.C., Caffee, M.W., Hudson, G.B., and Dietrich, W.E., 1997, Cosmogenic isotope analysis applied to river longitudinal profile evolution: Problems and interpretations: Earth Surface Processes and Landforms, v. 22, p. 195–209, doi: 10.1002/(SICI)1096-9837(199703)22:3<195::AID-ESP748>3.0.CO;2-0.

Selby, M.J., 1993, Hillslope Materials and Processes: New York, Oxford University Press, 451 p.

Stein, O.R., and Julien, P.Y., 1993, Criterion delineating the mode of headcut migration: Journal of Hydraulic Engineering, v. 119, no. 1, p. 37–50, doi: 10.1061/(ASCE)0733-9429(1993)119:1(37).

Stein, O.R., and LaTray, D.A., 2002, Experiments and modeling of headcut migration in stratified soils: Water Resources Research, v. 38, no. 12, doi: 10.1029/2001WR001166.

Tauxe, L., Luskin, C., Selkin, P., Gans, P., and Calvert, A., 2004, Paleomagnetic results from the Snake River Plain: Contribution to the time-averaged field global database: Geochemistry, Geophysics, Geosystems, v. 5, doi: 10.1029/2003GC000661.

Terzaghi, K., 1962, Stability of steep slopes in hard unweathered rock: Geotechnique, v. 12, p. 51–270.

Tómasson, H., 1973, Hamfarahlaup í Jökulsá a Fjöllum: Náttúrfrœðingurinn, v. 43, p. 12–34.

Unger, J.A., Faybishenko, B., Bodvarsson, G.S., and Simmons, A.M., 2004, Simulating infiltration tests in fractured basalt at the Box Canyon site, Idaho: Vadose Zone Journal, v. 3, p. 75–89.

Vischer, D.L., and Hager, W.H., 1995, Energy Dissipaters: Rotterdam, A.A. Balkema, 201 p.

Von Engeln, O.D., 1940, A particular case of knickpunkte: Annual Association of American Geography, v. 30, p. 268–271, 281–284.

Weissel, J.K., and Seidl, M.A., 1997, Influence of rock strength properties on escarpment retreat across passive continental margins: Geology, v. 25, no. 7, p. 631–634, doi: 10.1130/0091-7613(1997)025<0631:IORSPO>2.3.CO;2.

Welhan, J.A., and Reed, M.F., 1997, Geostatistical analysis of regional hydraulic conductivity variations in the Snake River Plain aquifer, eastern Idaho: Geological Society of America Bulletin, v. 109, no. 7, p. 855–868, doi: 10.1130/0016-7606(1997)109<0855:GAORHC>2.3.CO;2.

Whipple, K.X., and Tucker, G.E., 2002, Implications of sediment-flux–dependent river incision models for landscape evolution: Journal of Geophysical Research–Solid Earth, v. 107, no. B2, doi: 10.1029/2000JB000044.

Whipple, K.X., Hancock, G.S., and Anderson, R.S., 2000, River incision into bedrock: Mechanics and relative efficacy of plucking, abrasion, and cavitation: Geological Society of America Bulletin, v. 112, no. 3, p. 490–503, doi: 10.1130/0016-7606(2000)112<0490:RIIBMA>2.3.CO;2.

Williams, R.M.E., and Malin, M.C., 2004, Evidence for late stage fluvial activity in Kasei Valles, Mars: Journal of Geophysical Research, v. 109, E06001, doi: 10.1029/2003JE002178.

Wobus, C.W., Crosby, B.T., and Whipple, K.X., 2006, Hanging valleys in fluvial systems: Controls on occurrence and implications for landscape evolution: Journal of Geophysical Research–Earth Surface, v. 111, no. F2, doi: 10.1029/2005JF000406.

Wohl, E., 2008, The effect of bedrock jointing on the formation of straths in the Cache la Poudre River drainage, Colorado Front Range: Journal of Geophysical Research–Earth Surface, v. 113, no. F1, doi: 10.1029/2007JF000817.

Young, R., 1985, Waterfalls: Form and process: Zietschrift fur Geomorphologie, v. 55, N.F. Supplementband, p. 81–95.

Manuscript Received 12 June 2008
Revised Manuscript Received 5 September 2008
Manuscript Accepted 8 September 2008

Printed in the USA